J^* optimization of small aspect ratio stellarator/tokamak hybrid devices*

D. A. Spong,[†,a)] S. P. Hirshman, J. C. Whitson, D. B. Batchelor, B. A. Carreras, V. E. Lynch, and J. A. Rome
P.O. Box 2009, Oak Ridge National Laboratory, Oak Ridge, Tennessee 37830-8071

(Received 17 November 1997; accepted 10 February 1998)

A new class of low aspect ratio toroidal hybrid stellarators is found using a more general plasma confinement optimization criterion than quasisymmetrization. The plasma current profile and shape of the outer magnetic flux surface are used as control variables to achieve near constancy of the longitudinal invariant J^* on internal flux surfaces (quasiomnigeneity), in addition to a number of other desirable physics target properties. A range of compact (small aspect ratio A), low plasma current devices have been found with significantly improved confinement, both for thermal as well as energetic (collisionless) particle components. With reasonable increases in magnetic field and geometric size, such devices can also be scaled to confine 3.5 MeV alpha particle orbits.
[S1070-664X(98)95605-1]

I. INTRODUCTION

The three-dimensional nature of stellarator configurations offers a vast parameter space of possible design choices for plasma confinement systems. Attractive devices can now be identified out of this space due to the existence of efficient stellarator equilibrium algorithms[1] and multidimensional nonlinear optimization techniques[2] coupled with the development of relevant, but easily evaluated, physics target criteria. With respect to plasma transport, an essential advance[3] was the recognition that confinement depended only on the form of $|B|$ in a particular choice of a magnetic coordinate system. The structure of $|B|$ in this coordinate system can be directly controlled by the shape of the outer magnetic flux surface along with the plasma current and pressure profiles. These facts have allowed significant advances in the confinement quality of stellarator designs and, by allowing adequate confinement of deuterium-tritium (DT) fusion-produced alpha particles, made them credible as fusion power systems. However, most of these designs have remained at relatively high aspect ratios ($R_0/a>7$); the reactor embodiment of these devices then necessarily leads to large and expensive systems.

Low aspect ratio, modular-coil stellarator[4–8] designs have recently been developed that offer the attractive features of compact steady-state fusion power systems, high volume utilization, axisymmetric diverted regions, and the absence of low-order resonances (leading to islands) near the plasma edge. However, studies of confinement in these devices[6] have indicated a need for transport optimization. Of the two quasisymmetry approaches, only quasitoroidal optimizations have successfully been achieved[9] at low aspect ratio. The quasihelical approach[10] is expected to only be applicable at higher aspect ratios.[11] However, in parallel with the quasisymmetry approaches, various techniques for more directly targeting the drift of particle orbits away from magnetic flux surfaces have also been developed. An initial approach[12,13] in this direction was to focus specifically on improving the confinement of deeply trapped particles, since their orbits can simply be related to contours of the minimum of $|B|$ along the toroidal direction. We have developed a more general method that uses the alignment of the approximate second adiabatic invariant[14,15] J^* contours with magnetic flux surfaces. This allows confinement improvement over the entire trapped particle population as well as a reduction in the number of transitional particles. Such an approach is equivalent to bounce-averaged omnigeneity, which has recently been interpreted[16–18] in terms of equal spacing of $|B|$ contours on a magnetic flux surface. It has been demonstrated that this equal spacing of $|B|$ is both a necessary and sufficient condition for omnigeneity,[17] and that although quasihelical configurations are omnigenous, the class of nearly omnigenous configurations is much broader than that of quasihelical systems.[17] Besides allowing confinement improvement at a low aspect ratio,[19] this additional flexibility may be expected to better allow for the simultaneous optimization with respect to stability, bootstrap current profile, and other physics criteria. In the following we present an example of using the concept of bounce-averaged omnigeneity to generate an actual low aspect ratio stellarator configuration. Our new optimization procedure is first described, followed by an analysis of both the thermal and energetic particle transport properties of the optimized configuration. We find that sizable reductions (factors of $\approx$10–20) in thermal particle transport rates can be achieved along with a closing off of the loss cone for more energetic particles. Examination of the $|B|$ spectrum indicates that the optimized state is neither purely quasihelical nor quasitoroidal.

II. DESCRIPTION OF THE OPTIMIZATION PROCEDURE

Our approach uses the VMEC three-dimansional (3D) magnetohydrodynamic (MHD) equilibrium solver[1] aug-

*Paper cMoaI1-2 Bull Am. Phys. Soc. **42**, 1835 (1997).
[†]Invited speaker.
[a)]Electronic mail: spongda@ornl.gov

TABLE I. Components of stellarator optimization target χ^2 function.

Physics goal	Typical target criterion
B_{extrema} and drift and surfaces are aligned with flux surfaces (quasiomnigeneity). For J^* this is done for several values of ϵ/μ ranging from deeply trapped to nearly passing.	$B_{\min}=B_{\min}(\psi)$ $B_{\max}=B_{\max}(\psi)$ $J^*=J^*(\psi)$
Maintain fixed iota	e.g., $i(\psi)=0.3-0.2(\psi/\psi_{\max})$
Maintain magnetic well	$V''<0$
Target low aspect ratio	$R_0/a\approx 3$
Minimize magnetic ripple (decreases trapped particle fraction)	Minimize $(B_{\max}-B_{\min})$
Limit maximum plasma current	$\int_0^r r'dr' j_{\text{plasma}}(r')<I_{\max}$
Limit local magnetic surface curvature	Avoid strong elongation/cusps

mented with a transformation to Boozer coordinates,[3] as the inner physics evaluation loop of a Levenberg–Marquardt optimization algorithm. The control variables are the shape of the outermost magnetic flux surface, which is expressed in terms of about 20 Fourier harmonics of both R (the major radius) and z (the height above the midplane), and the plasma current profile. We have applied this optimization technique both to pure currentless stellarators as well as to hybrid systems, but find that the presence of plasma current offers greater flexibility and is generally necessary to attain high-β free boundary equilibria. Typically, the optimization targets used are the following: alignment of $B_{\min}$, $B_{\max}$, and J^* with magnetic flux contours; matching of $i(\psi)$ to a specified rotational transform profile; maintenance of a magnetic well over most of the plasma cross section; $R_0/a\approx 3$; avoidance of strongly curved segments on the flux surface; and minimization of magnetic ripple. The alignment of $B_{\min}$ with ψ improves the confinement of deeply trapped particles; alignment of $B_{\max}$ with ψ minimizes the number of transitional particles; alignment of J^* with ψ is applied over a range of pitch angles running from slightly above deeply trapped up to nearly passing in order to better confine the whole trapped particle population. We further include minimization of magnetic ripple in order to lower the number of trapped particles, since their confinement is not as good as passing particles (i.e., the alignment of the trapped J^* contours with ψ, although improved, is generally not exact). The avoidance of strongly curved segments on the flux surface is targeted in order to ease coil design and to avoid strongly elongated, narrow plasmas for which neutral penetration would be a problem. Our optimization procedure is quite flexible and can readily accommodate additional targets as the need arises. The currently used target criteria are summarized in Table I. Here $B_{\min}$ and $B_{\max}$, as used in the first and fifth target criteria of Table I, are the 2D functions of ψ and θ (i.e., magnetic flux and poloidal angle in Boozer coordinates) that are formed by recording the minimum/maximum value of $|B|$ along the toroidal direction within a single field period at fixed ψ, θ. The longitudinal invariant J^* is defined as follows:[14,15]

$$J^*(\psi,\theta)=\int_{\psi,\theta=\text{const}} \frac{g(\psi)d\phi}{B}\, m|v_\parallel|-\sigma_\parallel \frac{2\pi}{N}\psi_p,$$

with

$$\sigma_\parallel=\begin{cases} +1, & \text{copassing orbits,}\\ 0, & \text{locally trapped orbits } (v_\parallel=0 \text{ on orbit}),\\ -1, & \text{counterpassing orbits;}\end{cases}$$

where

$$v_\parallel=\pm\left[\frac{2}{m}(\epsilon-\mu B-q\Phi)\right]^{1/2}, \quad g(\psi)=\text{poloidal current},$$

ψ_p=poloidal magnetic flux function, N=number of field periods, ϵ=total energy, μ=magnetic moment, q=charge, and m=mass.

In general, J^* contours depend on ψ, θ, ϵ, ϵ/μ, and the electrostatic potential Φ. However, for our optimization approach, we shall only target trapped particles and the case where $\Phi=0$. In this limit, J^* only depends on ψ, θ, and ϵ/μ. For the examples given here, the alignment of the $B_{\min}$, $B_{\max}$, and trapped J^* contours with ψ is typically carried out over three or more flux surfaces and, additionally in the case of J^*, at four values of the pitch angle variable ϵ/μ (on a given flux surface, the trapped range of ϵ/μ is determined by $B_{\min,gl}<\epsilon/\mu<B_{\max,gl}$ where $B_{\min,gl}$ and $B_{\max,gl}$ are the global minima and maxima of $B_{\min}$ and $B_{\max}$ over the surface). Since the trapped branch of J^* is only defined over limited regions of each flux surface [i.e., running from $\theta_{\min}$ (the trapped/passing boundary at which $\epsilon/\mu=B_{\max}$) to $\theta_{\max}$ (the trapped/forbidden boundary at which $\epsilon/\mu=B_{\min}$)], its variation is only targeted within these boundaries. Each of the target functions in Table I is multiplied by an associated weight and summed to form a single χ^2 functional, which is to be minimized. The initial condition on the outer flux surface shape is either derived from a free-boundary VMEC equilibrium based on a known set of coils or from a previously optimized configuration.

Once a satisfactorily optimized outer flux surface is found, a second optimization procedure has been developed that varies a parametrized set of coils in order to match $\vec{B}$ at the outer flux surface. In general, this is not a unique process and multiple solutions are possible, depending on the number of coils per field period, the winding surface, etc. By separating the physics and coil optimizations into separate steps, efficiency is gained, the existence of flux surfaces is maintained during the optimization, and a better understanding of

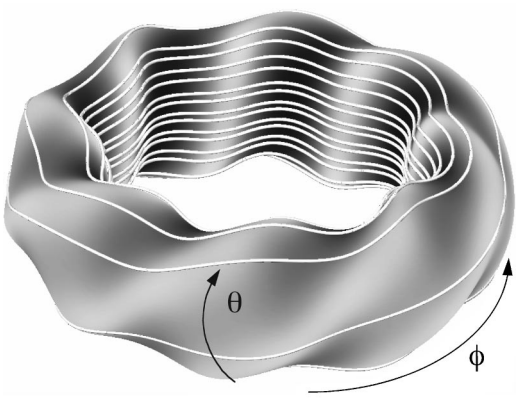

FIG. 1. Outer flux surface shape and magnetic field line (in white) with gray scale shading proportional to $|B|$ magnitude (the darker areas are higher field) for the J^*-optimized configuration.

the tradeoffs of each phase of the design process is possible. In the following, we will discuss only the physics (i.e., outer flux surface) optimization.

III. EXAMPLE OF AN OPTIMIZED CONFIGURATION

This optimization technique has been applied to an eight-field period, hybrid stellarator/tokamak device with major radius $R_0=1.3$ m, $B_{\text{axis}}=1.2$ T, $R_0/a\approx 2.8$, $\langle\beta\rangle=2\%$, and an integrated plasma current of around 60 kA. We will compare the initial unoptimized device, whose flux surface shape was determined by a set of eight external modular coils, with an optimized configuration based on the alignment of J^* with ψ. Figure 1 shows the 3D rendered flux surface for the optimized configuration with the gray scale shading used to indicate the constant $|B|$ contours. Also shown is a magnetic field line, indicating the strong poloidal variation in local transform that is characteristic of low aspect ratio stellarators. The variation of $|B|$ along a field line is shown in Fig. 2 for unoptimized, optimized, and equivalent tokamak configurations. The nearly constant minimum values of $|B|$ in the optimized configuration demonstrates the alignment of $B_{\min}$ contours with flux surfaces, which is achieved by the optimization. The iota profile in the unoptimized case increases from 0.22 at the center to 0.31 at $(\psi/\psi_{\max})^{1/2}=0.6$, and then drops to 0.15 at the edge while that of the optimized case drops from 0.4 at the center to 0.16 at $(\psi/\psi_{\max})^{1/2}=0.85$ and then increases to 0.2 at the edge. The integrated current profile of the unoptimized configuration increases monotonically to around 125 kA at the edge, while that of the optimized configuration increases to about 100 kA at $(\psi/\psi_{\max})^{1/2}=0.7$ and then drops to 60 kA at the edge [i.e., implying a reversed current density region outside of $(\psi/\psi_{\max})^{1/2}=0.7$]. Such profiles with regions of reversed edge current density have been characteristic of our optimizations, which target $di/dr<0$ and use the current profile as a control variable; the sensitivity of these optimizations to other current profile shapes will be examined in future work. Although the consistency of these profiles with bootstrap current drive has not been examined, compatible bootstrap current density profiles can, in principle, be maintained due to the fact that there is a difference in sign between the bootstrap current density driven in toroidally symmetrical regions and that driven in helically symmetrical regions. Our optimized case has low ripple levels near the center (toroidal symmetry), while at the edge it approaches helical symmetry. In Figs. 3(a) and 3(b) the J^* contours (for $\epsilon/\mu=1.08$—which is slightly above the deeply trapped limit) are shown for the two cases, indicating that the unoptimized configuration (a) has completely unclosed J^* contours (i.e., deeply trapped particles are lost), while the optimized configuration (b) has large regions of closed J^* contours. We have also examined the J^* contours over a range of pitch angles and find that they are more closely aligned with flux surfaces than in the original configuration.

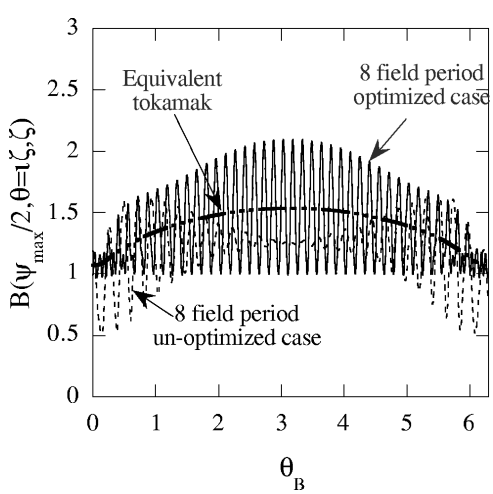

FIG. 2. Variation of $|B|$ along a field line on a flux surface at one-half the edge poloidal flux for the original unoptimized device (dashed line), the optimized device (solid line), and the equivalant tokamak (chain dashed line).

As mentioned earlier, the J^* optimization process leads to configurations that are neither quasitoroidal nor quasihelical. This is demonstrated in Figs. 4(a) and 4(b), where we have plotted $|B|$ versus toroidal and poloidal angles for an outer flux surface for (a) the unoptimized case and (b) the J^* optimized case. For a quasitoroidal system these contours would be horizontal lines, while for a quasihelical system they would be diagonal lines. As can be seen, our optimization in Fig. 4(b) does not fall into either category.

The approach to bounce-averaged omnigeneity through the alignment of trapped particle J^* surfaces with flux surfaces should be approximately equivalent to the criterion of equal angular separation between constant $|B|$ contours on a flux surface, which has been suggested recently in Refs. 16–18. The differences between these criteria are of order i/N (N=number of field periods) due to the difference between the exact J (the integral along a field line) and J^* (the integral along ϕ_{Boozer}) and are generally small for the configurations examined here. We have confirmed this by plotting contours of equal toroidal angle separation between a range of $|B|$ values and find that these contours are very similar to those of the equivalent J^* surfaces (i.e., at $\epsilon/\mu=|B|$).

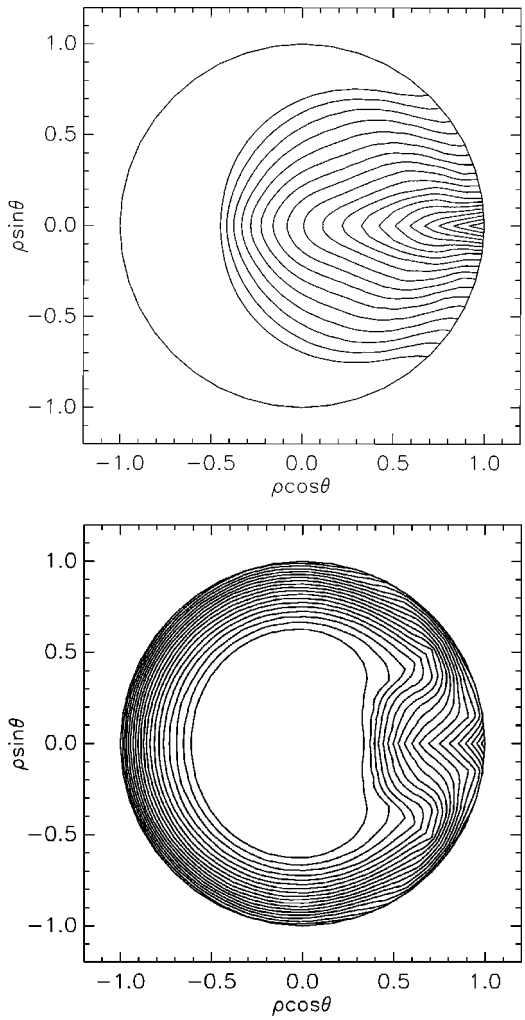

FIG. 3. The J^* contours at $\epsilon/\mu=1.08$ for (a) unoptimized and (b) J^*-optimized configurations.

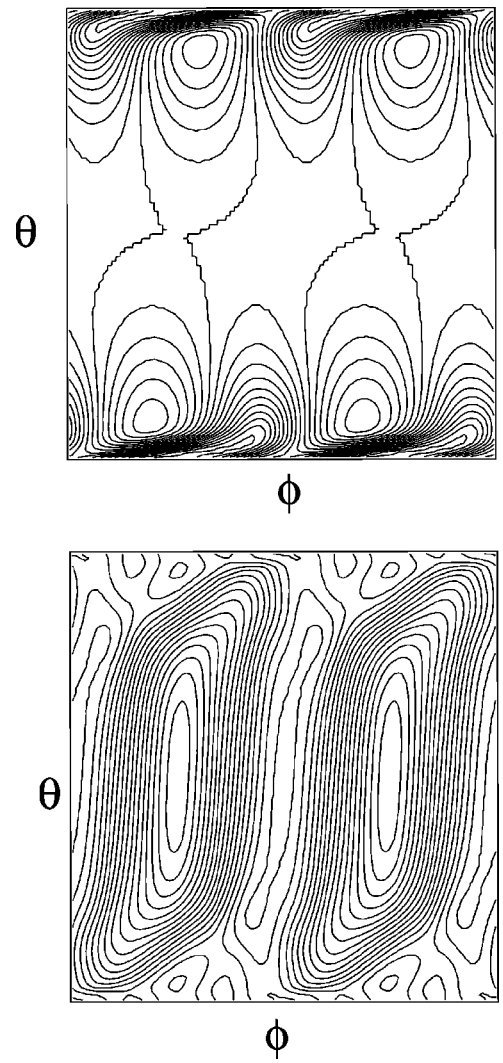

FIG. 4. The $|B|$ contours evaluated at the plasma edge for (a) the unoptimized case and (b) the J^*-optimized case.

IV. CONFINEMENT PROPERTIES OF THE OPTIMIZED CONFIGURATIONS

In conjunction with the above optimization process, it is important to use various measures to evaluate the optimized configurations. As the optimization will not generally lead to the precise alignment of J^* and magnetic flux surfaces, it is difficult to judge the relative merits of different optimized cases, simply by plotting the J^* contours. We have chosen to evaluate both the transport of thermal plasma and the confinement of energetic species (e.g., as required for plasma heating). Both of these measures are too time consuming to be incorporated directly into the optimization loop.

A. Thermal transport

In order to compare the thermal transport of the configurations presented in Sec. III, we have followed the Monte Carlo evolution[20] of 256 particles started at a single radial location ($\psi=0.25\psi_{\max}$), with a random distribution in pitch angle, poloidal and toroidal angles, and a monoenergetic distribution in energy. The background plasma has a density of 5×10^{13} cm^{-3} and a temperature of 1 keV; the test particle energy is also 1 keV. The ratio of the collision frequency to the bounce frequency is around 10^{-3}, placing the plasma in a regime where deeply trapped particles complete many bounces in the local ripple wells. The same random number seed was used for each configuration so that initial conditions are equivalent. We monitor the escape of particles and energy through the outer flux as a function of time and use this as our basic measure of thermal confinement. This loss rate has the advantage of including both the direct prompt orbit losses as well as diffusive losses and involves no assumptions regarding localized transport.

In Fig. 5 we show the particle loss rates versus time for the original, $B_{\min}$-optimized, and J^*-optimized cases along with an equivalent tokamak case. The latter configuration is arrived at from the J^*-optimized case by retaining only the $n=0$ harmonics. These results clearly demonstrate that the optimization procedure can substantially reduce loss rates, leading to about a factor of 10 reduction over the initial unoptimized configuration. The J^* optimized case is also within a factor of 3–4 of the equivalent tokamak loss rates.

A further interesting consequence of quasiomnigenous systems is that transport is not automatically ambipolar and

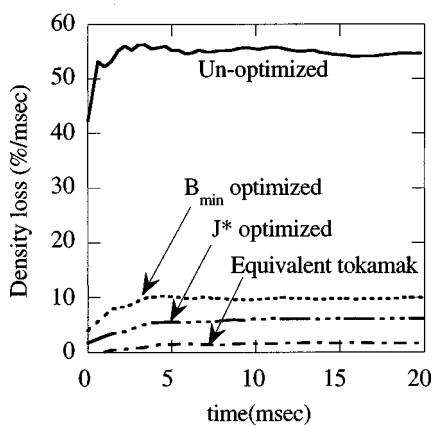

FIG. 5. The Monte Carlo particle loss rates through the last closed flux surface versus time for the original unoptimized configuration, a $B_{\min}$-optimized configuration, a J^*-optimized configuration, and an equivalent tokamak.

they therefore retain some degree of dependence of transport rates on the radial electric field. Quasisymmetric configurations should be isomorphic to tokamak transport,[21] which is independent of the electric field. In Fig. 6 we show examples of transport levels for the above J^*-optimized case in the presence of a potential profile that is zero at $r=0$ and rises near the plasma edge. As may be seen, moderate levels of the electric field can suppress density losses even below the equivalent tokamak level.

We next vary the background plasma density over the range of 10^{12}–10^{14} cm^{-3} to examine the collisionality scaling of transport for the J^*-optimized configuration (in this case with $e\phi/kT_{\rm ion}=0$). The results shown in Fig. 7 indicate that transport in the J^*-optimized configuration has a similar dependence as the tokamak and shows no evidence of a $1/\nu$ ripple transport regime. The unoptimized configuration also shows no indication of $1/\nu$ transport, possibly due to the fact that trapped orbits are directly lost on time scales ($\tau_{\rm loss}=0.2$–0.4 ms) less than that for collsions (0.17 ms$<\tau_{90}<7.5$ ms over the range of density considered here).

B. Energetic particle transport

The confinement of collisionless energetic particles is one of the primary motivations for the optimizations discussed here since the thermal particle confinement can, even without optimization, be improved by control of the ambipolar electric field.[6] Due to the fact that most heating schemes rely on some form of energetic particle tail population, heating efficiencies can depend sensitively on the confinement of this species.

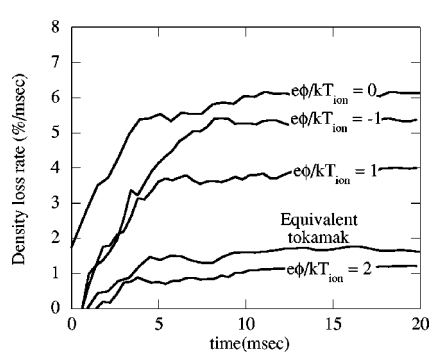

FIG. 6. Monte Carlo particle loss rates for the J^*-optimized case with various levels of a radial ambipolar electric field present.

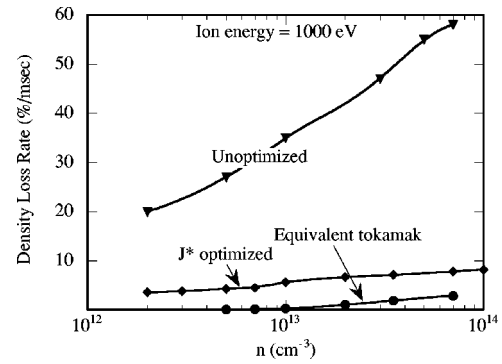

FIG. 7. The scaling of loss rates with density (collisionality) for the original unoptimized case, the J^*-optimized case (with $e\phi/kT_{\rm ion}=0$), and the equivalent tokamak case.

In order to compare the two configurations we have followed orbits at 40 keV that initially pass through the magnetic axis over a range of pitch angles and find that the unoptimized configuration has a loss cone over $-0.2<(v_\parallel/v)_0<0.4$. In contrast, the J^*-optimized configuration has no loss cone and confines the same orbits over the full range of $(v_\parallel/v)_0$. Besides confining the trapped orbits, the optimization also reduces the deviations of passing orbits away from flux surfaces. The deeply trapped orbits in the optimized configuration move on superbanana trajectories (i.e., banana-shaped orbits formed by many longitudinal bounces within a field period) and are confined up to energies at which their drift per bounce becomes too large for the longitudinal invariant J^* to be conserved. For the example configuration considered here, this occurs at around 400 keV. In Figs. 8(a) and 8(b), we display orbits in the J^*-optimized configuration with increasing energy for (a) a deeply trapped orbit $[(v_\parallel/v)_0=0.1]$ and (b) a copassing orbit $[(v_\parallel/v)_0=1.0]$ for energies of 100, 200, and 400 keV. The trapped orbit has lost confinement at around 400 keV. The passing orbits are still confined, but with significant displacements away from flux surfaces ($\Delta/a\approx 0.5$). The deeply trapped orbits show an interesting property of confined superbanana stellarator orbit trajectories in that, unlike normal tokamak banana orbits, the superbanana width is essentially independent of energy (i.e., due to the fact that for trapped particles and in the absence of electric fields J^* does not depend on energy). To the extent that J^* is conserved, relatively arbitrary energies will be confined on the same trajectory. The point at which J^* conservation is lost due to the drift per bounce becoming too large can be extended by increasing the B field or increasing the device size.

By scaling up the magnetic field and determining the maximum confined energy, we have predicted the increase in geometric size and magnetic field that would be required to confine 3.5 MeV alpha particles in our J^*-optimized example. In Fig. 9 the loss fraction of alphas is plotted as the

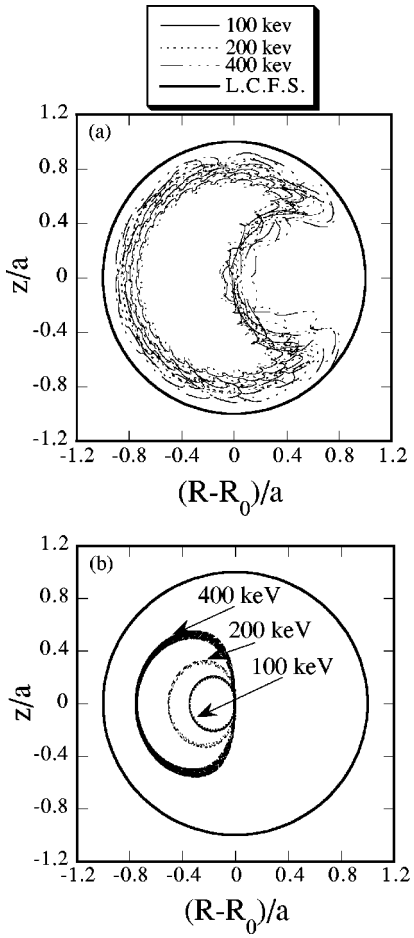

FIG. 8. Ion orbits that pass through the magnetic axis at 100, 200, and 400 keV in the J^*-optimized case for (a) $v_{\|0}/v=0.1$ (trapped) and (b) $v_{\|0}/v=1.0$ (passing).

energy is gradually increased. Here we have again only checked orbits passing through the magnetic axis and have scanned over the full range of pitch angles $-1<v_{\|0}/v<+1$. At a certain energy, the loss fraction rises steeply. Here f_B is the scale factor by which the magnetic field is increased. As f_B is increased, orbits can be confined at progressively higher energies. At around $f_B=4-5$, it becomes possible to confine a significant fraction ($\approx$90%) of 3.5 MeV alphas. This information can then be plotted in terms of the energy at which a specified level of loss occurs versus the

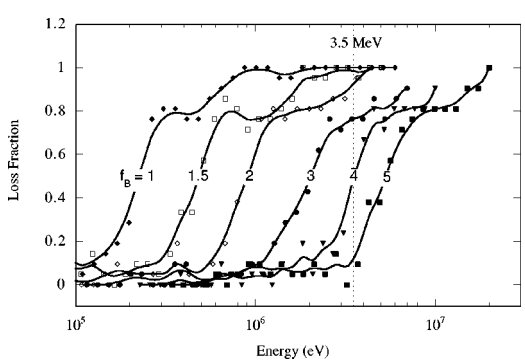

FIG. 9. Alpha particle loss fractions versus energy and scaling factor (f_B) in the product of size and magnetic field.

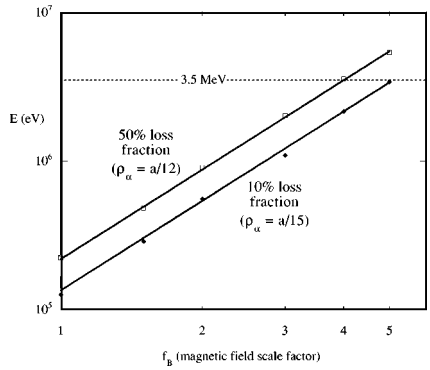

FIG. 10. The ρ_α/a scaling of various levels of alpha particle loss versus energy and f_B.

scaling factor, f_B, as shown in Fig. 10. For a fixed iota profile, both the drift per bounce (which determines the maximum energy of confined trapped orbits) as well the ratio of the displacement of passing orbits to the minor radius, scales as ρ/a, where ρ is the gyroradius. Figure 10 confirms this scaling (indicated by the straight lines) for both levels of loss up to at least 3.5 MeV. From these results, one could predict, for example, that if both the magnetic field and size were scaled up by a factor of $\approx$2 (recall that our initial device had $R_0=1.3$ m, $B_{\text{axis}}=1.2$ T, $R_0/a\approx 2.8$) one begins to confine a significant fraction of alphas. The plasma current in this example must also scale up with the product of size and magnetic field (a factor of 4–5) in order to maintain a fixed iota profile.

V. CONCLUSIONS

We have developed a new optimization procedure for low aspect ratio stellarators that targets bounce-averaged omnigeneity (i.e., minimization of drift away from the flux surface) by aligning contours of the approximate second adiabatic invariant J^* with magnetic flux surfaces. This technique uses the shape of the outermost flux surface and the plasma current profile as control parameters. Our optimization has led to qualitatively new kinds of stellarator configurations that are neither quasitoroidal nor quasihelical. This additional flexibility in the $|B|$ spectrum has opened up the available parameter space at low aspect ratio and resulted in significant improvements in confinement of both thermal as well as energetic particle components. For example, thermal transport can approach that of axisymmetric systems. We also find that with reasonable scale-ups in size and magnetic field, it is possible to confine 3.5 MeV alpha orbits. We expect that such flexibility will allow the inclusion of further criteria[22] related to MHD ballooning stability as well as other physics issues that may be of importance. Evaluations of ballooning stability in these configurations have already indicated that volume-averaged $\langle\beta\rangle$'s of 6% are stable. The coil reconstruction for these optimized states is relegated to a separate step and appears feasible, but will require further development.

ACKNOWLEDGMENT

This research was sponsored by the Office of Fusion Energy, U.S. Department of Energy, under Contract No. DE-AC05-960R22464.

[1]S. P. Hirshman and J. C. Whitson, Phys. Fluids **26**, 3553 (1983).
[2]P. E. Gill, W. Murray, and M. H. Wright, *Practical Optimization* (Academic, London, 1981).
[3]A. H. Boozer, Phys. Fluids **23**, 904 (1980).
[4]B. A. Carreras, N. Dominguez, L. Garcia, V. E. Lynch, J. F. Lyon, J. R. Cary, J. D. Hanson, and A. P. Navarro, Nucl. Fusion **28**, 1195 (1988).
[5]B. A. Carreras, V. E. Lynch, and A. Ware, ORNL/TM-13252, June, 1996, available through the NTIS (National Technical Information Service Springfield, VA 22161) as Document No. DE-96014592 for $19.50.
[6]D. A. Spong, S. P. Hirshman, and J. C. Whitson, Plasma Phys. Rep. **23**, 483 (1997).
[7]P. E. Moroz, Phys. Rev. Lett. **77**, 651 (1996).
[8]D. W. Ross, P. M. Valanju, H. He, W. H. Miner, P. E. Phillips, J. C. Wiley, A. J. Wooton, and S-B. Zheng, Plasma Phys. Rep. **23**, 492 (1997).
[9]P. R. Garabedian, Phys. Plasmas **3**, 2483 (1996).
[10]J. Nührenberg and R. Zille, Phys. Lett. A **129**, 113 (1988).
[11]D. A. Garren and A. H. Boozer, Phys. Fluids B **3**, 2822 (1991).
[12]R. N. Morris, C. L. Hedrick, S. P. Hirshman, J. F. Lyon, and J. A. Rome, *Proceedings of the 7th International Workshop on Stellarators*, Oak Ridge, TN, 10–14, April 1989 (International Atomic Energy Agency, Vienna, 1989).
[13]S. P. Hirshman, R. N. Morris, C. L. Hedrick, J. F. Lyon, J. A. Rome, S. L. Painter, W. I. Van Rij, in Ref. 12.
[14]J. R. Cary, C. L. Hedrick, and J. Tolliver, Phys. Fluids **31**, 1586 (1988).
[15]J. A. Rome, Nucl. Fusion **35**, 195 (1995).
[16]A. A. Skovoroda and V. D. Shafranov, Plasma Phys. Rep. **21**, 886 (1995).
[17]J. R. Cary and S. G. Shasharina, Phys. Rev. Lett. **78**, 674 (1997).
[18]H. Weitzner, Phys. Plasmas **4**, 575 (1997).
[19]S. P. Hirshman, D. A. Spong, J. C. Whitson, D. B. Batchelor, B. A. Carreras, V. E. Lynch, and J. A. Rome, Phys. Rev. Lett. **80**, 528 (1998).
[20]R. H. Fowler, J. A. Rome, and J. F. Lyon, Phys. Fluids **28**, 338 (1985).
[21]A. H. Boozer, Phys. Fluids **26**, 496 (1983).
[22]W. A. Cooper, Phys. Plasmas **4**, 153 (1997).